

Optical response of threaded chain plasmons: from capacitive chains to continuous nanorods

Christos Tserkezis,¹ Lars O. Herrmann,² Ventsislav K. Valev,² Jeremy J. Baumberg,² and Javier Aizpurua^{1,*}

¹*Donostia International Physics Center (DIPC) and Centro de Física de Materiales (CFM) CSIC-UPV/EHU, Paseo Manuel de Lardizabal 4, Donostia-San Sebastián, 20018, Spain*

²*Nanophotonics Centre, Cavendish Laboratory, Department of Physics, JJ Thomson Avenue, University of Cambridge, Cambridge, CB3 0HE, UK*

*aizpurua@ehu.es

Abstract: We present a detailed theoretical analysis of the optical response of threaded plasmonic nanoparticle strings, chains of metallic nanoparticles connected by cylindrical metallic bridges (threads), based on full-electrodynamic calculations. The extinction spectra of these complex metallic nanostructures are dominated by large resonances in the near infrared, which are associated with charge transfer along the entire string. By analysing contour plots of the electric field amplitude and phase we show that such strings can be interpreted as an intermediate situation between metallic nanoparticle chains and metallic nanorods, exhibiting characteristics of both. Modifying the dielectric environment, the number of nanoparticles within the strings, and the dimensions of the threads, allows for tuning the optical response of the strings within a very broad region in the visible and near infrared.

© 2014 Optical Society of America

OCIS codes: (250.5403) Plasmonics; (160.4236) Nanomaterials; (350.4990) Particles.

References and links

1. J. N. Anker, W. P. Hall, O. Lyandres, N. C. Shah, J. Zhao, and R. P. Van Duyne, "Biosensing with plasmonic nanosensors," *Nature (London) Mater.* **7**, 442–453 (2008).
2. H. Chen, G. C. Schatz, and M. A. Ratner, "Experimental and theoretical studies of plasmon-molecule interactions," *Rep. Prog. Phys.* **75**, 096402 (2012).
3. A. G. Brolo, "Plasmonics for future biosensors," *Nature (London) Photon.* **6**, 709–713 (2012).
4. R. Zhang, Y. Zhang, Z. C. Dong, S. Jiang, C. Zhang, L. G. Chen, L. Zhang, Y. Liao, J. Aizpurua, Y. Luo, J. L. Yang, and J. G. Hou, "Chemical mapping of a single molecule by plasmon-enhanced Raman scattering," *Nature (London)* **498**, 82–86 (2013).
5. D. Darvill, A. Centeno, and F. Xie, "Plasmonic fluorescence enhancement by metal nanostructures: shaping the future of bionanotechnology," *Phys. Chem. Chem. Phys.* **15**, 15709–15726 (2013).
6. J. A. Schuller, E. S. Barnard, W. Cai, Y. C. Jun, J. S. White, and M. L. Brongersma, "Plasmonics for extreme light concentration and manipulation," *Nature (London) Mater.* **9**, 193–204 (2010).
7. M. I. Stockman, "Nanoplasmonics: past, present, and glimpse into future," *Opt. Express* **19**, 22029–22106 (2011).
8. N. I. Zheludev and Y. S. Kivshar, "From metamaterials to metadevices," *Nature (London) Mater.* **11**, 917–924 (2012).
9. Z. Fang and X. Zhu, "Plasmonics in nanostructures," *Adv. Mater.* **25**, 3840–3856 (2013).
10. M. Kauranen and A. V. Zayats, "Nonlinear plasmonics," *Nature (London) Photon.* **6**, 737–748 (2012).
11. X. Zhang, Y. L. Chen, R.-S. Liu, and D. P. Tsai, "Plasmonic photocatalysis," *Rep. Prog. Phys.* **76**, 046401 (2013).

12. A. Alù and N. Engheta, "Plasmonic and metamaterial cloaking: physical mechanisms and potentials," *J. Opt. A: Pure Appl. Opt.* **10**, 093002 (2008).
13. C. M. Soukoulis and M. Wegener, "Past achievements and future challenges in the development of three-dimensional photonic metamaterials," *Nature (London) Photon.* **5**, 523–530 (2011).
14. A. Christofi, N. Stefanou, G. Gantzoounis, and N. Papanikolaou, "Giant optical activity of helical architectures of plasmonic nanorods," *J. Phys. Chem. C* **116**, 16674–16679 (2012).
15. V. K. Valev, J. J. Baumberg, C. Sabilia, and T. Verbiest, "Chirality and chiroptical effects in plasmonic nanostructures: fundamentals, recent progress, and outlook," *Adv. Mater.* **25**, 2517–2534 (2013).
16. J. Pérez-Juste, I. Pastoriza-Santos, L. M. Liz-Marzán, and P. Mulvaney, "Gold nanorods: synthesis, characterization, and applications," *Coord. Chem. Rev.* **249**, 1870–1901 (2005).
17. L. J. Sherry, S.-H. Chang, G. C. Schatz, R. P. Van Duyne, B. J. Wiley, and Y. Xia, "Localized surface plasmon resonance spectroscopy of single silver nanocubes," *Nano Lett.* **5**, 2034–2038 (2005).
18. E. Carbó-Argibay, B. Rodríguez-González, J. Pacífico, I. Pastoriza-Santos, J. Pérez-Juste, and L. M. Liz-Marzán, "Chemical sharpening of gold nanorods: the rod-to-octahedron transition," *Angew. Chem. Int. Ed.* **46**, 8983–8987 (2007).
19. F. Hao, C. L. Nehl, J. H. Hafner, and P. Nordlander, "Plasmon resonances of a gold nanostar," *Nano Lett.* **7**, 729–732 (2007).
20. L. R. Hirsch, A. M. Gobin, A. R. Lowery, F. Tam, R. A. Drezek, N. J. Halas, and J. L. West, "Metal nanoshells," *Ann. Biomed. Eng.* **34**, 15–22 (2006).
21. S. J. Tan, M. J. Campolongo, D. Luo, and W. Cheng, "Building plasmonic nanostructures with DNA," *Nature (London) Nanotech.* **6**, 268–276 (2011).
22. E. Ringe, B. Sharma, A.-I. Henry, L. D. Marks, and R. P. Van Duyne, "Single nanoparticle plasmonics," *Phys. Chem. Chem. Phys.* **15**, 4110–4129 (2013).
23. H. Tamaru, H. Kuwata, H. T. Miyazaki, and K. Miyano, "Resonant light scattering from individual Ag nanoparticles and particle pairs," *Appl. Phys. Lett.* **80**, 1826–1828 (2002).
24. K.-H. Su, Q.-H. Wei, X. Zhang, J. J. Mock, D. R. Smith, and S. Schultz, "Interparticle coupling effects on plasmon resonances of nanogold particles," *Nano Lett.* **3**, 1087–1090 (2003).
25. E. Prodan, C. Radloff, N. J. Halas, and P. Nordlander, "A hybridization model for the plasmon response of complex nanostructures," *Science* **302**, 419–422 (2003).
26. P. Nordlander, C. Oubre, E. Prodan, K. Li, and M. I. Stockman, "Plasmon hybridization in nanoparticle dimers," *Nano Lett.* **4**, 899–903 (2004).
27. H. Xu, J. Aizpurua, M. Käll, and P. Apell, "Electromagnetic contributions to single-molecule sensitivity and in surface-enhanced Raman scattering," *Phys. Rev. E* **62**, 4318–4324 (2000).
28. E. Hao and G. C. Schatz, "Electromagnetic fields around silver nanoparticles and dimers," *J. Chem. Phys.* **120**, 357–366 (2004).
29. S. S. Aćimović, M. P. Kreuzer, M. U. González, and R. Quidant, "Plasmon near-field coupling in metal dimers as a step toward single-molecule sensing," *ACS Nano* **3**, 1231–1237 (2009).
30. I. Romero, J. Aizpurua, G. W. Bryant, and F. J. García de Abajo, "Plasmons in nearly touching metallic nanoparticles: singular response in the limit of touching dimers," *Opt. Express* **14**, 9988–9999 (2006).
31. K. J. Savage, M. M. Hawkeye, R. Esteban, A. G. Borisov, J. Aizpurua, and J. J. Baumberg, "Revealing the quantum regime in tunnelling plasmonics," *Nature (London)* **491**, 574–577 (2012).
32. J. A. Scholl, A. García-Etxarri, A. L. Koh, and J. A. Dionne, "Observation of quantum tunneling between two plasmonic nanoparticles," *Nano Lett.* **13**, 564–569 (2013).
33. T. Atay, J.-H. Song, and A. V. Nurmikko, "Strongly interacting plasmon nanoparticle pairs: from dipole-dipole interaction to conductively coupled regime," *Nano Lett.* **4**, 1627–1631 (2004).
34. O. Pérez-González, N. Zabala, A. G. Borisov, N. J. Halas, P. Nordlander, and J. Aizpurua, "Optical spectroscopy of conductive junctions in plasmonic cavities," *Nano Lett.* **10**, 3090–3095 (2010).
35. M. Quinten, A. Leitner, J. R. Krenn, and F. R. Aussenegg, "Electromagnetic energy transport via linear chains of silver nanoparticles," *Opt. Lett.* **23**, 1331–1333 (1998).
36. S. A. Maier, M. L. Brongersma, P. G. Kik, and H. A. Atwater, "Observation of near-field coupling in metal nanoparticle chains using near-field polarization spectroscopy," *Phys. Rev. B* **65**, 193408 (2002).
37. A. F. Koenderink and A. Polman, "Complex response and polariton-like dispersion splitting in periodic metal nanoparticle chains," *Phys. Rev. B* **74**, 033402 (2006).
38. A. Alù and N. Engheta, "Theory of linear chains of metamaterial/plasmonic particles as subdiffraction optical nanotransmission lines," *Phys. Rev. B* **74**, 205436 (2006).
39. S. J. Barrow, A. M. Funston, D. E. Gómez, T. J. Davis, and P. Mulvaney, "Surface plasmon resonances in strongly coupled gold nanosphere chains from monomer to hexamer," *Nano Lett.* **11**, 4180–4187 (2011).
40. T. Chen, M. Pourmand, A. Feizpour, B. Cushman, and B. M. Reinhard, "Tailoring plasmon coupling in self-assembled one-dimensional Au nanoparticle chains through simultaneous control of size and gap separation," *J. Phys. Chem. Lett.* **4**, 2147–2152 (2013).
41. R. Esteban, R. W. Taylor, J. J. Baumberg, and J. Aizpurua, "How chain plasmons govern the optical response in strongly interacting self-assembled metallic clusters of nanoparticles," *Langmuir* **28**, 8881–8890 (2012).

42. C. Tserkezis, R. W. Taylor, J. Beitner, R. Esteban, J. J. Baumberg, and J. Aizpurua, "Optical response of metallic nanoparticle heteroaggregates with subnanometric gaps," *Part. Part. Syst. Charact.* **31**, 152–160 (2014).
43. Z. Li, S. Butun, and K. Aydin, "Touching gold nanoparticle chain based plasmonic antenna arrays and optical metamaterials," *ACS Photon.* **1**, 228–234 (2014).
44. L. O. Herrmann, V. K. Valev, C. Tserkezis, J. S. Barnard, S. Kasera, O. A. Scherman, J. Aizpurua, and J. J. Baumberg, "Threading plasmonic nanoparticle strings with light," *Nature (London) Commun.* **5**, 4568 (2014).
45. R. W. Taylor, T.-C. Lee, O. A. Scherman, R. Esteban, J. Aizpurua, F. M. Huang, J. J. Baumberg, and S. Mahajan, "Precise subnanometer plasmonic junctions for SERS within gold nanoparticle assemblies using cucurbit[*n*]uril "glue"," *ACS Nano* **5**, 3878–3887 (2011).
46. F. J. García de Abajo and J. Aizpurua, "Numerical simulation of electron energy loss near inhomogeneous dielectrics," *Phys. Rev. B* **56**, 15873–15884 (1997).
47. F. J. García de Abajo and A. Howie, "Retarded field calculation of electron energy loss in inhomogeneous dielectrics," *Phys. Rev. B* **65**, 115418 (2002).
48. P. B. Johnson and R. W. Christy, "Optical constants of the noble metals," *Phys. Rev. B* **6**, 4370–4379 (1972).
49. O. Pérez-González, N. Zabala, and J. Aizpurua, "Optical characterization of charge transfer and bonding dimer plasmons in linked interparticle gaps," *New J. Phys.* **13**, 083013 (2011).
50. Y. Wang, Z. Li, K. Zhao, A. Sobhani, X. Zhu, Z. Fang, and N. J. Halas, "Substrate-mediated charge transfer plasmons in simple and complex nanoparticle clusters," *Nanoscale* **5**, 9897–9901 (2013).
51. G. W. Bryant, F. J. García de Abajo, and J. Aizpurua, "Mapping the plasmon resonances of metallic nanoantennas," *Nano Lett.* **8**, 631–636 (2008).
52. L. Novotny, "Effective wavelength scaling for optical antennas," *Phys. Rev. Lett.* **98**, 266802 (2007).
53. J. Aizpurua, G. W. Bryant, L. J. Richter, F. J. García de Abajo, B. K. Kelley, and T. Mallouk, "Optical properties of coupled metallic nanorods for field-enhanced spectroscopy," *Phys. Rev. B* **71**, 235420 (2005).

1. Introduction

The field of plasmonics has experienced tremendous growth during the past decade thanks to significant advances in nanotechnology and nanofabrication. Novel plasmonic nanoparticles and their aggregates can be exploited for example in (bio)sensing, towards the limit of single-molecule sensing, enhanced fluorescence signals, localised surface plasmon resonance sensing or surface- and tip-enhanced Raman scattering [1–5]. Complex planar or periodic plasmonic architectures have been proposed for the design of optoelectronic devices, such as waveguides, photodectors, filters, modulators, switches, and spasers [6–9]. In addition, plasmonic nanostructures trigger and enhance nonlinear phenomena, which further facilitate optoelectronic applications [10]. Light energy harvesting, photovoltaics and photocatalysis have also benefited from plasmonics [6, 9, 11], while negatively refracting or chiral metamaterials and optical cloaking devices use plasmonic nanoparticles as their main building blocks in the visible [12–15].

The simplest and most easily accessible plasmonic nanostructure is the single metallic nanoparticle. Starting from the simplest nanoparticle, i.e., the metallic nanosphere, and gradually increasing anisotropy, introducing faceting, edges or additional layers, a great variety of plasmonic nanoparticles have been fabricated, the most common of which are metallic nanorods [16], nanocubes [17], polyhedra [18], nanostars [19], and nanoshells [20]. A detailed presentation of different fabricated nanoparticle shapes can be found in Refs. [21, 22]. The next step towards a more elaborate plasmonic functionality and optical response is to bring two of these nanoparticles in close proximity, to form nanoparticle dimers [23, 24]. The interaction between the plasmon modes of the individual particles leads to new, hybrid plasmon modes, known as Bonding Dimer Plasmon (BDP) modes [25, 26], and very high field enhancements within the interparticle gaps, referred to as electromagnetic (EM) hot spots [27–29].

When the distance between particles in a plasmonic dimer is reduced towards the touching regime, new phenomena occur. As the particles approach each other, their interaction leads to significant redshifting of the hybrid plasmon modes and diverging EM field enhancement within the hot spots according to classical electrodynamics [30]. In reality, for interparticle gaps smaller than about 0.5 nm, quantum mechanical effects including electron tunnelling become important [31, 32]. This quantum mechanical charge transfer between the particles leads to

saturation of the mode redshifting or even disappearance of the hybrid BDP modes, which are replaced by Charge Transfer Plasmon (CTP) modes, while the near-field enhancement becomes finite. CTP modes can of course be excited in a dimer in a simpler manner, by bringing the two nanoparticles into contact [30, 33, 34].

Another strategy to increase complexity and obtain a richer optical response from plasmonic nanoparticles is by designing larger aggregates of such particles. One of the simplest geometries is a linear chain of nanoparticles [35–40]. In such chains, long-wavelength modes associated with collective plasmon excitations along the entire chain dominate the optical spectra [41, 42]. Here, we proceed one step further in designing conducting chain-like plasmonic geometries, by allowing charge transfer along the nanoparticle chains, and therefore combining the chain plasmons with CTPs. A theoretical study of chains of metallic nanospheres with a single touching point was presented recently [43]. Here, we follow a different approach, by creating gold threads, that is, cylindrical bridges of well-defined dimensions to connect the spheres in a nanoparticle string. Such strings were recently fabricated by ultrafast-laser irradiation [44] of cucurbituril-assisted self-assemblies characterised by robust chain plasmon modes [41, 45]. We analyse the far-field spectra of threaded strings in comparison to those of plasmonic dimers, and examine the dependence of the modes on the number of particles forming the strings, their dielectric environment, and the dimensions of the threads connecting the particles. We then discuss the nature of the different modes as deduced from their respective near fields. Finally, we show that there is a continuous transition, determined by the width of the metallic threads, from an unthreaded chain of metallic nanoparticles to a metallic nanorod. These metallic nanoparticle strings can be exploited as efficient, tunable nanoantennas in the infrared, or as building blocks for novel nano- or meta-materials.

Throughout the paper, far-field extinction spectra, and near-field amplitude and phase maps are calculated by numerical simulations using the full electrodynamic boundary-element method (BEM) [46, 47]. The BEM method solves Maxwell's equations for inhomogeneous media characterised by local dielectric functions in terms of surface-integral equations of the induced charges and currents, which are obtained through discretisation of the surface integrals and solution of the resulting matrix equations. The EM field is then calculated in terms of these induced charges and currents. In order to ensure full convergence of the results, 2 points per nm at each interface were used for the discretisation of the circumference of the spheres, while 15 points per nm were used for the accurate description of the threads. With use of these criteria, convergence of all the results was achieved.

2. Capacitive chain plasmons and threaded chain plasmons

Let us first briefly discuss the nature of the modes dominating the spectra of unthreaded and threaded gold nanosphere dimers. In Fig. 1(a) we show the extinction (σ_{ext}) spectrum of an unthreaded dimer (black dashed curve). The dimer consists of two gold nanospheres, described by the dielectric function of Johnson and Christy [48], with diameter $D = 40$ nm, separated by a gap with length $l = 1$ nm, in air, and it is illuminated by a plane wave described by a wavevector \mathbf{k} and an electric field \mathbf{E} with amplitude E_0 , polarised along the dimer axis (taken to be the z axis), as shown schematically on the top of the figure. The main feature is a resonance at wavelength $\lambda = 560$ nm, which is reshifted with respect to the surface plasmon resonance of the individual gold nanospheres (at 520 nm). This resonance is a hybrid dipolar BDP mode, originating from the interaction of the plasmon modes of the two nanoparticles in close proximity. The BDP mode corresponds to in-phase surface charge oscillations in both particles, along the dimer axis. The two nanoparticles can be described as two coupled parallel electric dipoles. Reducing the distance between the nanoparticles leads to efficient excitation of higher order hybrid modes [26, 30].

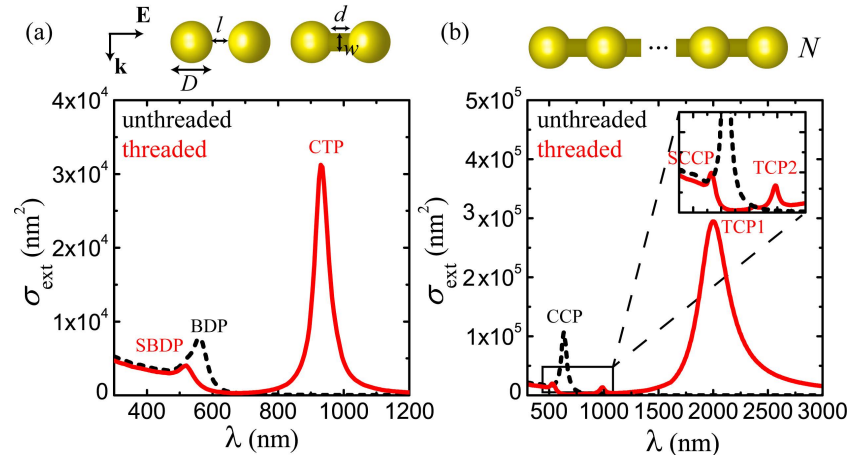


Fig. 1. (a) Extinction (σ_{ext}) spectra for the unthreaded (black dashed curve) and the threaded (red solid curve) gold nanoparticle dimers in air shown schematically on top. The dimers consist of two gold nanospheres with diameter $D = 40$ nm, separated by a 1-nm gap, and are illuminated by a plane wave polarised along the dimer axis. The gold thread connecting the two nanospheres is modelled as a cylinder with length $d = 1$ nm and diameter $w = 10$ nm. (b) Extinction spectra of an unthreaded chain consisting of $N = 8$ gold nanospheres ($D = 40$ nm) (black dashed curve) and the corresponding threaded nanoparticle string (red solid curve) shown schematically on top ($d = 1$ nm, $w = 10$ nm) in air, illuminated by a plane wave polarised along the chain axis.

We now add a thread to connect the two nanoparticles. The thread is modelled as a gold cylinder with diameter w , and length $d = 1$ nm in its centre and increasing towards the circumference, so as to fully contact the spheres at the touching points, as shown in the right-hand schematic of Fig. 1(a). The thread between the two spheres ($w = 10$ nm in Fig. 1(a)) allows charge transfer between them, leading to the appearance of a new mode at $\lambda = 930$ nm, which is associated with charge oscillations along the entire dimer. This is the CTP discussed in Refs. [34, 49, 50]. At the same time, the BDP mode blueshifts, towards 520 nm, and the electric field is expelled from the thread. Since the interaction of charges at the cavity is screened due to the presence of the thread, this mode is now called the Screened BDP (SBDP) [34]. We should note that, depending on the dimensions and the conductivity of the thread (if it is made of a different material), the SBDP mode can either redshift or blueshift [49].

Long metallic nanoparticle chains behave in a similar way: in the unthreaded chain, a long-wavelength mode, typically between 600 and 800 nm, dominates the spectrum, as shown by the black curve in Fig. 1(b) for a chain of $N = 8$ spheres in air. This mode, which in our case appears at $\lambda = 635$ nm, is associated with a collective plasmon excitation of the nanoparticles forming the chain, which behaves like a long electric dipole [41, 42]. We call this resonance the Capacitive Chain Plasmon (CCP) [44], since the coupling between the particles is a capacitive one. The CCP has essentially the same nature as the BDP in a dimer. Once metallic threads are introduced to produce a nanoparticle string, the CCP mode blueshifts, decreases in intensity and becomes a Screened CCP (SCCP) mode, similarly to the behaviour of the BDP in a dimer. The spectrum is now dominated by a much more intense mode in the infrared, as shown in Fig. 1(b) for threads with $w = 10$ nm, which we label as the first order Threaded Chain Plasmon (TCP1) [44]. This mode is associated with charge transfer along the entire nanoparticle string, and has therefore the same nature as the CTP of a dimer: for a threaded dimer, CTP and TCP1

are identical. A second mode, with lower intensity, appears between the CCP and TCP1 modes, and is more clearly shown in the inset of Fig. 1(b). As we discuss later in more detail, this is the second order TCP mode (TCP2 in Fig. 1(b)). We should also note that, since the screened modes, SBDP and SCCP, evolve naturally from BDP and CCP respectively for non-zero thread conductance, in the rest of the paper we omit the term screened and refer to them as the BDP and CCP.

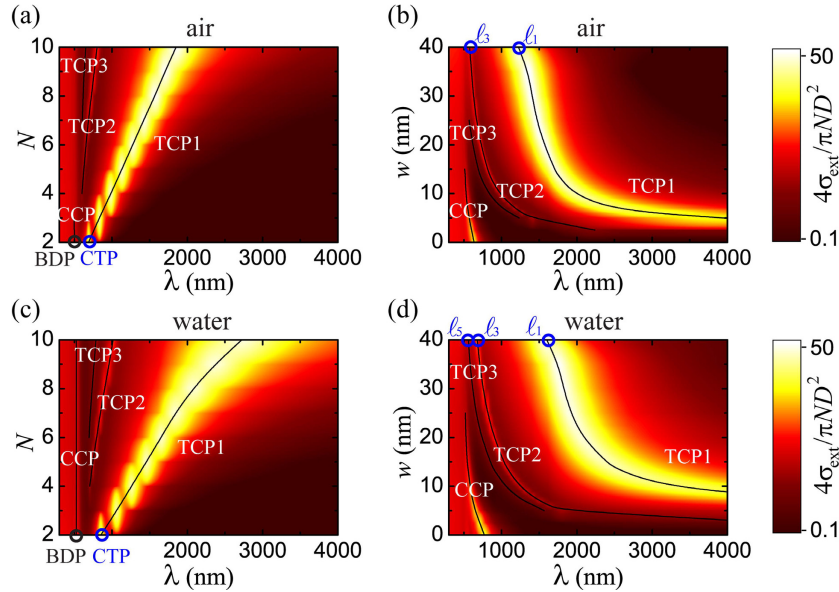


Fig. 2. (a) Contour plots (on logarithmic scale) of the extinction cross section, normalised to the geometric cross section $\pi N(D/2)^2$, for gold nanoparticle strings consisting of $N = 2$ to 10 nanospheres ($D = 40$ nm, $w = 20$ nm), in air. The contour serves as a guide to the eye: only values for integer N have a physical meaning. (b) Contour plots (on logarithmic scale) of the extinction cross section, normalised to the geometric cross section $\pi N(D/2)^2$, for a string consisting of eight 40-nm nanospheres, as a function of thread width w , in air. (c) Same as (a), in water. (d) Same as (b), in water. In all contour plots, the black lines trace the resonance peaks of the modes. Black and blue circles in (a) and (c) mark the BDP and CTP modes, respectively. Blue circles in (b) and (d) mark the nanorod antenna modes.

Since the TCP modes originate from charge transfer along the entire nanoparticle string, it is expected that their optical properties will depend strongly on the number of particles forming the strings. In order to study this effect, in Fig. 2 we analyse contours of the extinction cross section, normalised to the geometric cross section per sphere, $\pi N(D/2)^2$, where N is the number of spheres in each string (ignoring for simplicity the much smaller contribution from the threads). In Fig. 2(a) we maintain the thread width constant, $w = 20$ nm, and increase the number of nanoparticles, from two to ten. As N increases, the TCP1 mode redshifts strongly, without a tendency to saturate with string length. This is contrary to the case of unthreaded nanoparticle chains [41,42], but in good agreement with what is expected for a perfect metallic rod of increasing length [51,52]. The CTP of the dimer, as described in Fig. 1(a), is the limiting case of TCP1 for $N = 2$, and is marked by a blue circle at the bottom of Fig. 2(a). Similarly, the BDP mode of the dimer is the limiting case of the CCP of the chain for $N = 2$, and is labelled by a black circle. Higher-order TCP modes (TCP2 and TCP3 in the figure) are efficiently excited only when the string is long enough to support them, a behaviour which is again similar to that

of a metallic nanorod [51, 53].

The energy of the TCP modes is strongly dependent on the properties of the threading bridge. In Fig. 2(b) we show the dependence of the modes on the width of the thread, for an eight-nanoparticle string. For unthreaded chains only the CCP mode appears, as expected. As a thread is formed, TCP modes are gradually also excited. When the threads are too narrow, less than about 2.5 nm, charge transfer is not strong enough, the thread conductance is too low, and the TCP modes appear in the extinction spectra as very weak, broad peaks at very long wavelengths in the infrared (not shown in Fig. 2(b)), until, for very thin threads, they disappear completely [34]. Following a simple model presented in Refs. [34, 49], we can evaluate the conductance required for the TCP mode to appear, G_{TCP} , as

$$G_{\text{TCP}} = \frac{c}{8\lambda_{\text{TCP}}} \frac{D^2}{d}, \quad (1)$$

where c is the velocity of light in vacuum and λ_{TCP} is the wavelength at which the TCP mode first emerges. According to our simulations, for the strings studied in Fig. 2(b) λ_{TCP} is approximately equal to 5000 nm. Using the conductance obtained from Eq. (1) we can then estimate the critical thread width, w_{TCP} , for the emergence of the TCP mode as [49]

$$w_{\text{TCP}}^2 = \frac{4d}{\pi} \frac{G_{\text{TCP}}}{\kappa}, \quad (2)$$

where κ is the conductivity of gold at λ_{TCP} . This leads to a critical thread width equal to 1.2 nm, a value which is close to the results of our simulations, thus extending the validity of the concept of conductance threshold from dimers [34, 49] to nanoparticle strings. As the threads become broader, easier paths for charge transfer among the nanoparticles are established and the TCP modes become more intense and start blueshifting. The CCP mode, on the other hand, blueshifts and loses intensity, until it eventually reaches the spectral regime dominated by the interband transitions of gold, and cannot be distinguished any more. Finally, for thread widths equal to the diameter of the particles, a perfect continuous metallic rod is formed, and the TCP modes become the odd antenna modes (ℓ_1, ℓ_3 , etc.) [53] marked by blue circles at the upper part of Fig. 2(b).

Although the main modes characterising the strings are already visible in Figs. 2(a) and 2(b), the higher-order modes (TCP2, TCP3) appear only as very small peaks in the visible or near infrared, very close to the CCP mode. It is therefore useful to modify the dielectric environment to distinguish their evolution. For that purpose, we consider an environment of water (described by a dielectric constant equal to 1.77). This is a reasonable choice, since the strings can be experimentally fabricated from self-assembled aggregates in aqueous solutions [44]. Increasing the refractive index contrast leads to strong redshifting of the modes, as can be seen both in Fig. 2(c) and 2(d), where again, the modal dependence on particle number and thread width is presented. The spectral split between the different modes is clearer in this situation, therefore in the rest of the paper we choose water as the surrounding medium of the strings. Comparison between Figs. 2(a) and 2(c), or 2(b) and 2(d), shows the large refractive index sensitivity of these modes, which, for the TCP1 mode and relatively long chains ($N = 10$ in Fig. 2), can be as large as 650-700 nm/RIU (RIU: refractive index unit), although the large width of the modes leads to low figures of merit, of the order of 3-4.

In order to show the nature of the TCP modes more clearly, we present in Fig. 3 contour plots of the normalised electric field amplitude, $|E/E_0|$, and the phase of the electric field component parallel to the string axis (z axis), ϕ_{E_z} , for a string consisting of eight nanospheres connected by 15-nm wide threads, in water. The extinction spectrum of this string is shown in Fig. 3(a) on a logarithmic scale, so that all the modes are clearly visible. The corresponding contour plots

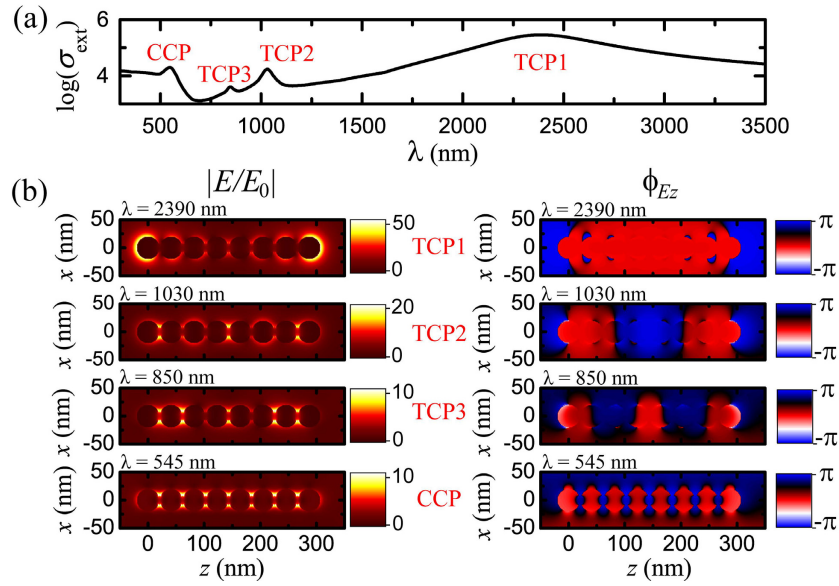


Fig. 3. (a) Extinction cross section (on logarithmic scale) for a gold nanoparticle string ($w = 15$ nm) consisting of eight 40-nm nanospheres in water. (b) From top to bottom: contours of the normalised electric field amplitude ($|E/E_0|$, left contours) and the phase of the electric field component parallel to the string axis (ϕ_{Ez} , right contours), at the wavelengths of TCP1 ($\lambda = 2390$ nm), TCP2 ($\lambda = 1030$ nm), TCP3 ($\lambda = 850$ nm), and CCP ($\lambda = 545$ nm), for the gold nanosphere string of (a).

for each mode are shown in Fig. 3(b). The TCP1 mode has clearly a predominantly dipolar character, with strong near-field enhancement at the two edges of the string, as shown in the left-hand contour plot. In addition, smaller, but still relevant field enhancements are also produced around each thread, and are accompanied by crevices of opposite phase, which imply strong surface charge densities, as can be seen in the right-hand-side plot of the phase. The largest field enhancement is obtained in this case around the midmost thread. Apart from the additional charges around the threads, the field profile of TCP1 of the string is similar to that of a metallic nanorod for its ℓ_1 mode [53]. In a similar manner, the TCP2 and TCP3 modes exhibit the characteristics of the nanorod ℓ_3 and ℓ_5 modes, as can be seen especially in the phase contour plots of Fig. 3(b). Additional strong near-field enhancements at the gaps (around the threads) can also be observed. Again, the highest field enhancement around a thread occurs at the middle of regions of the same phase ϕ_{Ez} , at the maximum or minimum of the electric field oscillation. This behaviour allows us to conclude that the TCP modes described here are novel hybrid modes, which mix a nanorod character, allowed due to the connections made by the threads, with the in-gap field enhancement observed for the CCP modes of unthreaded chains. On the other hand, the near field of the hybrid CCP mode (bottom contour plots in Fig. 3(b)) resembles that of an unthreaded chain [41, 42], where all the particles forming the chain have similar field distributions around them. However, since gold now occupies the centres of the interparticle gaps, the electric field is expelled from the threads, and the field enhancement becomes significantly smaller, localised only at the sides of the threads.

As we discussed above, the near-field profiles of the threaded nanoparticle strings exhibit a strong nanorod character. Thus it is interesting to explore in more detail the dependence of these modes on thread width, and particularly, to examine the width at which the nanorod

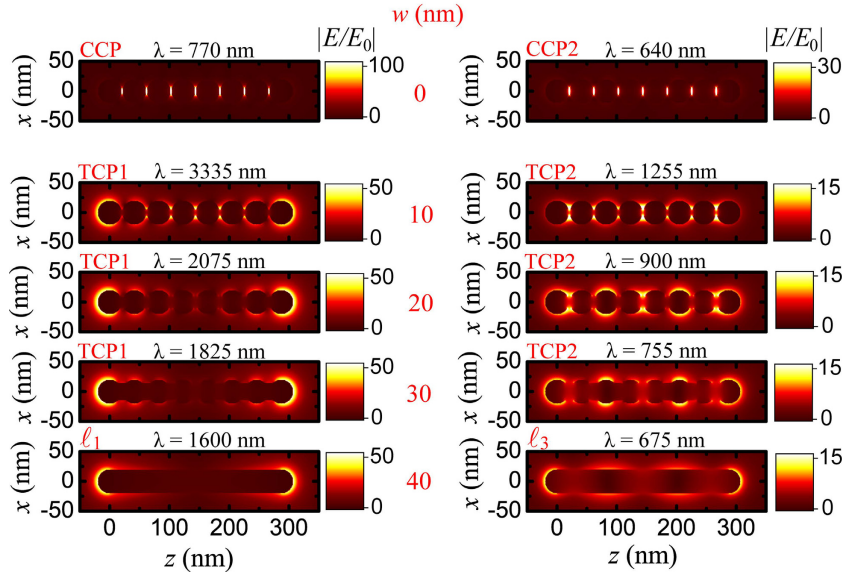


Fig. 4. Contour plots of the normalised electric field amplitude for a chain of eight 40-nm nanospheres in water, as the thread increases from $w = 0$ nm (unthreaded chain, top contours), to $w = 40$ nm (perfect nanorod, bottom contours), for the TCP1 (left contours) and the TCP2 (right contours) modes.

character is first expressed. In Fig. 4 we show maps of $|E/E_0|$ and ϕ_{Ez} for the two first TCP modes (TCP1, left, and TCP2, right) as the thread width increases. For $w = 0$ nm (the case of an unthreaded chain) TCP modes are not excited. Instead, we show the first two CCP modes, CCP and CCP2, of the unthreaded chain, which have very high electric field enhancement at the capacitive gaps as their main characteristic (top contour plots). We should note here that for the eight-nanoparticle chains considered here, CCP2 appears only as a small shoulder near CCP in the extinction spectrum, and is not discernible in Fig.3(a). However, it is clearly visible in corresponding near-field spectra [41, 42]. For the other limiting case, of large thread width, equal to the nanosphere diameter ($w = 40$ nm), we obtain the field profiles of perfect metallic nanorods, and the TCP1 and TCP2 modes become the antenna ℓ_1 and ℓ_3 modes, respectively (bottom contour plots). In all the intermediate, threaded string cases, the electric field distribution follows exactly the trends of the nanorod, with the maxima and minima occurring at the same positions. Additional large field enhancements, which decrease as the threads become wider, appear around the threads, as we discussed in relation to Fig. 3. This rod-like character is already clear for thread widths equal to 10 nm. Our simulations showed that this transition from a chain to a rod already starts for threads as thin as 5 nm, which highlights the importance of the established charge transfer paths to build the modes. In this way, the electric field contours of the threaded strings can be seen as a superposition of the field patterns of the two limiting cases (unthreaded chain and nanorod).

3. Conclusion

In summary, we theoretically studied the optical properties of threaded metallic nanoparticle strings made of chains of metallic nanospheres connected by cylindrical metallic bridges (threads). We showed that, when metallic threads are introduced to connect metallic nanoparticles in a string-like chain, the CCP modes of the chain blueshift as the thread widens, their

intensity is reduced and the optical response of the strings is progressively dominated by TCP modes in the near infrared. The TCP modes are hybrid chain/rod modes, which have a predominant antenna (rod-like) character, while strong field enhancements around the threads are also produced. The wavelength of the TCP modes depends strongly on the dielectric environment, the number of particles in the chains, and the dimensions of the threads, which allows their efficient tuning within a wide range in the visible and near infrared. We have shown that plasmonic nanoantennas with a rich and tuneable optical response in the infrared can be obtained by threading the particles, serving as building blocks of complex nanooptical devices and metamaterials

Acknowledgments

CT and JA acknowledge financial support from Project FIS2013-41184-P of the Spanish Ministry of Economy and Competitiveness (MINECO), project ETORTEK 2014-15 of the Department of Industry of the Basque Government, and from the Department of Education of the Basque Government, IT756-13 of consolidated groups. LOH, VKV, and JJB acknowledge financial support from EPSRC grants EP/K028510/1, EP/G060649/1, EP/H007024/1, EP/L027151/1 and ERC LINASS 320503.